

DRAG REDUCTION AND SHAPE OPTIMIZATION OF AIRSHIP BODIES

Th. Lutz* and S. Wagner†

Institute for Aerodynamics and Gas Dynamics
University of Stuttgart, Germany

Abstract. A tool for the numerical shape optimization of axisymmetric bodies submerged in incompressible flow at zero incidence has been developed. Contrary to the usual approach, the geometry of the body is not optimized in a direct way with this method. Instead, a source distribution on the body axis was chosen to model the body contour and the corresponding inviscid flowfield, with the source strengths being used as design variables for the optimization process. Boundary-layer calculation is performed by means of a proved integral method for attached laminar or turbulent boundary layers. To determine the transition location, a semi-empirical method based on linear stability theory (e^n -method) was implemented recently. A commercially available optimizer as well as an evolution strategy with covariance matrix adaption of the mutation distribution are applied as optimization algorithms. Shape optimizations of airship hulls were performed with this new tool for different Reynolds number regimes. The objective was to minimize the drag for a given volume of the envelope and a prescribed airspeed range. The results obtained show a high sensitivity of the optimization result towards the transition criterion used.

Nomenclature

A	amplitude of a Tollmien-Schlichting wave
c_d	drag coefficient
c_{d_v}	volumetric drag coefficient
D	drag
f	frequency
$H_{1,2}$	shape factor
n	amplification factor
N	total number of source sections
q_{0_i}	source strength at the beginning of the i^{th} section
q_{1_i}	source strength at the end of the i^{th} section
r_{0_i}	distance from start of i^{th} source section to field point
r_{1_i}	distance from end of i^{th} source section to field point
Re	Reynolds number
Re_L	Reynolds number based on body length
Re_V	volumetric Reynolds number
Re_{δ_1}	Reynolds number based on δ_1
s	arc length
t	time
U_∞	undisturbed freestream velocity
V	body volume
w_x	axial velocity component
w_r	radial velocity component
x, r	coordinates of the cylindrical coordinate system

α_r	wave number
α_i	amplification rate
δ_1	displacement thickness
Δx_i	length of i^{th} source section
φ	eigenfunction
ν	kinematic viscosity
Φ	velocity potential
ρ	density of the fluid
ω	circular frequency

Indices

A	field point
crit.	critical value
I	value at the primary instability point
V	quantity based on body volume

1 Introduction

In the process of developing new airships, the central topics are presently reliable construction and safe operation. If in the future airships for long endurance missions or for transportation purposes are realised, the factor of economical operation will become of greater interest. It will then be most important to minimize the weight and the power requirements of the configuration. The propulsive power required depends mainly on the aerodynamic drag of the airship hull, which accounts for about 2/3 of the total drag. Even a small reduction in hull drag can result in a significant saving of fuel, which in turn will lead to a greater payload capacity or an increased range of the airship. During the aerodynamic design of an airship it is therefore especially important to find a drag-minimized envelope for the intended range of missions.

Apart from the shape optimization of the bare hull, additional aspects should be addressed. For example the moment gradient of the envelope plays an important role for the total drag of the configuration, since it determines the size of the fins required to achieve a desired level of static stability. For an actual airship project it will furthermore be necessary to find a drag-minimized shape with the center of buoyancy within a specified range and a favourable hull surface to volume ratio in order to minimize the hull mass.

Previous Research on Low-Drag Bodies

First systematical investigations on the drag of axisymmetric bodies were conducted by Gertler [7]. The objective of his experimental work was the determination of a low-drag submarine contour. Since no extensive laminar flow regions were expected for this application, no special laminar bodies have been investigated in this research study.

* Research Assistant

† Professor, Head of Institute, Member AIAA.

The question concerning drag reduction by extended laminar flow at medium Reynolds numbers was investigated by Carmichael by means of drop-tests carried out in the Pacific Ocean [2]. He was able to prove that for $Re_L=10$ to $40 \cdot 10^6$ extensive laminar flow is possible. For the body examined (fineness ratio $L/D=3.33$), a reduction of the volumetric drag coefficient of up to 60 % could be achieved compared to conventional turbulent body shapes.

Further experimental research on laminar bodies for low Reynolds number applications was conducted by Hansen & Hoyt [9]. The low drag coefficients expected from theoretical calculations could be confirmed experimentally for this Reynolds number regime. During the experiments a high sensitivity of the transition location to even the smallest surface roughness was observed, which restricts practical applications of such extensively laminar bodies.

Experimental investigations on the drag of axisymmetric bodies at large Reynolds numbers ($Re_V > 10^7$), relevant for airship applications, are hardly known. Therefore, mainly theoretical methods have to be relied on. First numerical shape optimizations were performed by Parsons et al. [16]. The calculation method is based on a panel code which was coupled with a boundary-layer method. Eight parameters were chosen as design variables to represent the body geometry.

In contrast Zedan et al. [28] used an inverse method based on a linearly varying doublet distribution on the body axis for the design of low-drag aircraft fuselages. The fuselage designed shows a long region with a favourable pressure gradient in its forward part. It was stated that this should result in laminar flow up to 70 % of the body length at Reynolds numbers of $Re_V=10$ to $30 \cdot 10^6$. Further numerical shape optimizations were carried out for example by Dodbele et al. [4], Coiro et al. [3] or Pinebrook [17].

Most publications on shape optimization concern the design of bodies with extended laminar flow. An exception in this respect is the research done by Hess, who conducted drag computations for bodies of revolution where the boundary layer is fully turbulent [10]. His disillusioning conclusion was that the drag is very insensitive to changes in body contour and thus that no significant drag reduction can be obtained from shaping alone in case of a fully turbulent boundary layer.

In [13] and [14] shape optimizations of axisymmetric bodies were presented by the authors. In order to carry out these investigations, a calculation method had been developed which is based on the coupling of an indirect potential method with an integral boundary-layer method and an evolution strategy as optimization algorithm (see [24]). At Reynolds numbers below $Re_V=10^7$ extensive laminar flow regions could be theoretically achieved, which results in a very low volumetric drag coefficient, even if compared to known laminar bodies. In the range of very large, airship-relevant Reynolds numbers ($Re_V \gtrsim 10^7$) the laminar flow regions achievable by shaping alone proved to be short, as expected. The shape optimizations conducted for this high Reynolds number regime did not result in significant drag reduction.

Because of the small amount of computing time required, an empirical local transition criterion was used with the shape optimizations presented in [13] and [14]. Analysis of the optimized geometries by means of a more sophisticated e^n -method for transition prediction resulted partly in considerably different transition locations and confirmed the inadequacies of local criteria [14]. For this reason, a costly e^n -method based on linear stability theory has also been implemented recently in the optimization tool. The extensions and improve-

ments in the aerodynamic calculation model and in the optimization algorithm will be described hereafter. Up-to-date optimization results for different Reynolds number regimes will then be presented and discussed.

2 Flow Calculation about Axisymmetric Bodies at Zero Incidence

For the present investigations potential-flow methods have been coupled with a boundary-layer code to calculate the drag of bodies of revolution at zero incidence. During the shape optimization process, the inviscid flow field is computed by means of an efficient inverse method based on a linearly varying source distribution on the body axis. In contrast, a three-dimensional panel method is used to analyse the flow about given body shapes. Drag evaluation is performed by means of an integral method for attached laminar or turbulent boundary layers. The same method is used during the design as well as during the analysis calculation. Special emphasis is laid on the determination of the transition point, since the length of the laminar flow region has a substantial impact on the drag coefficient especially for small to medium Reynolds numbers. A transition prediction method as reliable and consistent as possible is of essential importance for successful shape optimization of laminar bodies. The transition criterion employed will therefore be discussed in more detail.

2.1 Inviscid Formulation

Design Procedure

Based on the assumption of an isentropic and, aside from possible singular points, irrotational flow field, a velocity potential Φ can be introduced. Thereby the total potential Φ consists of the potential of the undisturbed onset flow and the perturbation potential caused by the body. The continuity equation supplies the equation for the determination of the velocity potential, which assumes the form of the Laplace equation in case of an incompressible fluid:

$$\Delta\Phi=0 \quad (1)$$

As this potential equation represents a partial *linear* differential equation, a superposition of elementary solutions is possible. These basic solutions include for example a parallel flow or the flow field of a source or a doublet singularity. The flow about a body of revolution at zero incidence can be modeled by superimposing the flow field of a source distribution on the body axis with that of a parallel onset flow in axial direction. In order to generate closed body contours, the closure condition has to be satisfied. This condition implies that the integral of the source strength has to be zero at the body tail. The present approach uses a source distribution varying linearly by section, as proposed by Pinebrook [17], see Fig. 1. The total potential in an arbitrary field point $A(x,r)$, resulting from the parallel onset flow and the influence of all N source segments, is then given by:

$$\begin{aligned} \Phi_A = & u_\infty x + \\ & - \frac{1}{4\pi} \sum_{i=1}^N \frac{1}{\Delta x_i} \left\{ (q_{1_i} - q_{0_i})(r_{1_i} - r_{0_i}) + \right. \\ & \left. + [q_{1_i}(x - x_{0_i}) - q_{0_i}(x - x_{1_i})] \ln \kappa \right\} \end{aligned} \quad (2)$$

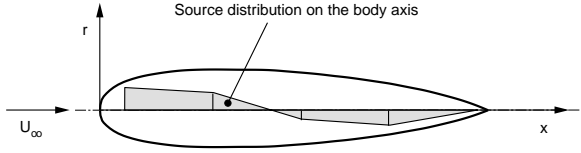


Figure 1. Modeling of flow field and geometry of an axisymmetric body at zero incidence by means of a source distribution on the body axis

$$\text{where } \kappa = \frac{x - x_{0i} + r_{0i}}{x - x_{1i} + r_{1i}}$$

Here, q_{0i} represents the source strength at the beginning, q_{1i} the source strength at the end and Δx_i the length of the i^{th} segment, see Fig. 2. The distance between field point A and the beginning or end of the source segment is designated by r_{0i} or r_{1i} respectively.

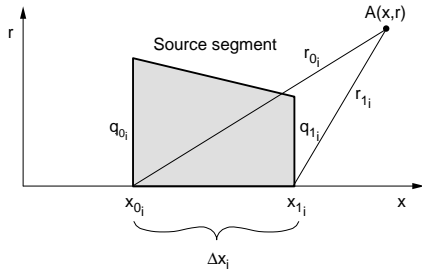


Figure 2. Source section with linearly varying strength

For a given source distribution the inviscid velocity field results from the differentiation of the total potential. Thus, the axial resp. radial velocity component at an arbitrary field point $A(x, r)$ follows from Eq. (2):

$$\begin{aligned} w_{x_A} &= \frac{\partial \Phi_A}{\partial x} \\ &= u_\infty - \frac{1}{4\pi} \sum_{i=1}^N \left[\frac{q_{0i}}{r_{0i}} - \frac{q_{1i}}{r_{1i}} + \frac{q_{1i} - q_{0i}}{\Delta x_i} \ln \kappa \right] \end{aligned} \quad (3)$$

$$\begin{aligned} w_{r_A} &= \frac{\partial \Phi_A}{\partial r} \\ &= \frac{1}{4\pi} \sum_{i=1}^N \frac{1}{\Delta x_i} \left\{ (q_{1i} - q_{0i}) \left(\frac{1}{r_{0i}} - \frac{1}{r_{1i}} \right) \right. \\ &\quad \left. + [q_{1i}(x - x_{0i}) - q_{0i}(x - x_{1i})] \right. \\ &\quad \left. \left[\frac{1}{r_{0i}(x - x_{0i} + r_{0i})} - \frac{1}{r_{1i}(x - x_{1i} + r_{1i})} \right] \right\} \end{aligned} \quad (4)$$

Due to the rotational symmetry of the flow field with the two independent variables x and r a stream function can be introduced whose definition is such that the continuity equation is fulfilled identically. The value of the stream function Ψ_A in the field point $A(x, r)$ for the singularity distribution chosen results in:

$$\begin{aligned} \Psi_A &= \int w_{x_A} r \, dr \\ &= \frac{u_\infty}{2} r^2 - \frac{1}{4\pi} \sum_{i=1}^N \frac{1}{\Delta x_i} \left\{ (q_{1i} - q_{0i}) r^2 \ln \kappa + \right. \\ &\quad \left. + [q_{1i}(x - x_{0i}) - q_{0i}(x + x_{0i} - 2x_{1i})] r_{0i} \right. \\ &\quad \left. + [q_{0i}(x - x_{1i}) - q_{1i}(x + x_{1i} - 2x_{0i})] r_{1i} \right\} \end{aligned} \quad (5)$$

The body contour is finally given by the stagnation stream surface. The defining equation for the body contour is therefore obtained by setting Eq. (5) equal to the value of the stream function in the stagnation points. For a given singularity distribution, the geometry can be calculated from the defining equation by means of an iterative procedure.

For a prescribed source distribution the potential method described above enables a very simple and efficient calculation of the body contour and the corresponding inviscid flow field. The approach is, however, restricted to axisymmetric bodies at zero incidence submerged in incompressible fluid. Because of its computational efficiency, this indirect method is used within the shape optimization process. Thereby, the source strengths at the segment boundaries and the corresponding segment lengths are chosen as design variables (see Section 3.2).

It should be emphasised that not all imaginable body shapes can be modeled with this inverse method. For example, bodies with a length-to-diameter ratio smaller than one have to be excluded. Such blunt, separation-prone bodies will not be discussed in the scope of this paper due to their inferior aerodynamic characteristics. Zedan [27] concluded that any axisymmetric low-drag shape found in current literature can be modeled by means of a singularity distribution on the body axis.

Analysis Procedure

To solve the direct problem, i. e. to calculate the inviscid velocity distribution for given body shapes, a three-dimensional panel method is applied. In this analysis method source singularities with panelwise constant strength are used, with the singularity distribution being determined by application of the external Neumann boundary-condition. This low-order approach is sufficient when using an adequately fine discretization of the body geometry. A modified Bezier spline serves for the interpolation of geometry and velocity distribution and provides the input data for the boundary-layer calculation. If required, the displacement effect of the boundary layer can be simulated by means of the transpiration technique, which will necessitate an iterative coupling with the boundary-layer method.

2.2 Boundary-Layer Method

The boundary-layer calculation is performed based on the inviscid velocity distribution on the body surface which results from the design or analysis procedure described above. For the present investigations, an integral method according to Eppler [6] has been applied, which enables the efficient calculation of attached laminar or turbulent two-dimensional boundary layers. This code was expanded for the calculation of axisymmetric boundary layers. The method is based on the

numerical integration of the integral form of momentum and energy equation. The additionally required closure relations were derived from the similar solutions of the boundary-layer equations in the case of laminar boundary layers. For turbulent boundary layers, empirical relations are used.

Curvature effects are neglected with the first-order method. This simplification seems permissible, because the boundary-layer thickness in the Reynolds number range investigated is much smaller than the curvature radii. An exception to this is the area right around the body tail.

In the original method the laminar to turbulent transition is determined by means of an empirical local transition criterion. For the present investigations this local criterion was replaced by a semi-empirical e^n -method based on linear stability theory, which will be described in more detail in the following section.

If laminar separation occurs upstream of transition, the method switches to turbulent boundary-layer calculation at the separation point. The additional drag arising due to laminar separation bubbles is not accounted for. The drag coefficient is determined by using the formula of Young [26], which takes the skin friction and form drag of attached boundary layers into account. In the implementation considered here boundary-layer data is evaluated at each coordinate point in the region of attached turbulent flow in order to determine a local value of the drag coefficient. The maximum of these values is then attributed to represent the drag coefficient of the examined body of revolution.

2.3 Transition Prediction

Various authors refer to the deficiencies of simple local transition criteria for the evaluation of the transition point of airfoil sections and axisymmetric bodies (see e. g. [4], [5], [25], [28]). Especially for slender bodies with a flat pressure distribution a wide range of transition locations can be found with different criteria. This results from the fact that local criteria take the boundary-layer development and the involved transition mechanisms only insufficiently into account. The scope of these empirical criteria is therefore limited, and they show relatively large scattering in comparison to wind-tunnel measurements (see e. g. [25]).

Transition from Laminar to Turbulent Boundary-Layer Flow

At a low freestream turbulence level, the boundary layer starting at the stagnation point is at first laminar and stable against perturbations. Downstream of a certain point, the so-called primary instability point, disturbance waves with small amplitude (Tollmien-Schlichting waves) are being amplified, i. e. their amplitude grows in downstream direction. After this region of linear instability non-linear interaction of different disturbance waves occur. This secondary instability initiates the subsequent stages of the transition process, which lead to a rapid breakdown to turbulence. The detailed transition process will not be discussed any further in this paper.

The amplification of sinusoidal disturbance waves of small amplitude can be computed by means of the linear stability theory in very good agreement with experimental results. Because the region of non-linear perturbation-wave amplification is short if compared to the region of linear instability, this theory can be used to derive predictions about the transition

location by so-called semi-empirical transition criteria, such as the e^n -method.

Linear Stability Theory for Two-Dimensional, Incompressible Boundary Layers

The first basic assumption of the linear stability theory is to separate the two-dimensional boundary-layer flow into a steady basic flow $U(y)$ and an unsteady disturbance. Furthermore, local parallelism is assumed. The basic flow represents a steady solution of the Navier-Stokes equation, whereas for the disturbance a harmonic wave approach is chosen, which can be described by means of the following stream function:

$$\Psi = \varphi(y) e^{i(\alpha x - \omega t)} + \text{complex conjugate} \quad (6)$$

In this equation, y represents the distance normal to the wall. The perturbation velocity components in streamwise and normal direction result from differentiation of the stream function.

Substitution of the disturbance velocities into the complete Navier-Stokes equation, elimination of the pressure variable and linearization result in the Orr-Sommerfeld equation, which can be expressed in the following form:

$$(D^2 - \alpha^2)^2 \varphi = i \alpha Re \left[\left(U - \frac{\omega}{\alpha} \right) (D^2 - \alpha^2) - D^2 U \right] \varphi \quad (7)$$

$$\text{where } D = \frac{d}{dy}$$

Here we consider spatial growth of the Tollmien-Schlichting waves. In this case, ω represents a real quantity and stands for the circular frequency of the disturbance waves. In contrast, α is complex with its real part being the wavenumber α_r and its imaginary part being the amplification rate α_i . Negative values for α_i indicate a spatial amplification whereas positive values mean decay of the perturbation wave amplitude.

Since the boundary conditions for the above equation (no-slip condition at the wall, vanishing perturbation wave amplitude at infinity) are homogeneous, an eigenvalue problem results. Now the amplitude development of a Tollmien-Schlichting wave with circular frequency ω can be evaluated for a given boundary-layer profile of the steady basic flow and specified local Reynolds number.

The linear stability theory, as described above, has been derived for two-dimensional flow. Since within the present investigations the boundary-layer thickness is much smaller than the radius over the entire body, this approach can be applied for axisymmetric boundary layers as well.

Semi-Empirical e^n -Method for Transition Prediction

Smith & Gamberoni [21] and independently van Ingen [22] first developed a semi-empirical transition criterion based on linear stability theory. With this e^n -method the transition from laminar to turbulent flow is assumed, when the amplification factor n for a certain frequency has reached a critical value n_{crit} :

$$n = \ln \frac{A}{A_I} = - \int_{s_I}^s \alpha_i(f) ds \geq n_{crit}. \quad (8)$$

In this equation, $\frac{A}{A_1}$ describes the ratio of the local amplitude A of the Tollmien-Schlichting waves to the amplitude A_1 in the primary instability point s_1 . The critical amplification factor is assumed to be dependent on the freestream conditions (turbulence level, sonic disturbances). Based on comparisons of experimentally found and theoretically obtained transition locations, Mack [15] and van Ingen [23] presented correlations for $n_{crit.}$ depending on the freestream turbulence level. Note that the process of receptivity and the magnitude of the initial disturbance amplitude is not considered. Furthermore the method fails if large-amplitude perturbations enter the boundary layer and the linear stages of the transition process are bypassed.

In the implementation presented here, the boundary-layer profiles required for the computation of the amplification rates are obtained from a polynomial approximation of the Falkner-Skan profiles. This approach is practical, since the laminar boundary-layer method used is based on the similar solutions of the boundary-layer equations. For a specified family of profiles, stability analysis can be performed in advance to find a non-ambiguous relation between the local Reynolds number $Re_{\delta_{1l}}$ and the shape factors H_{12l} or H_{32l} at the primary instability point. This relation can be used to evaluate the location of the primary instability point within actual transition calculations. Stability analysis then only has to be performed downstream of this point.

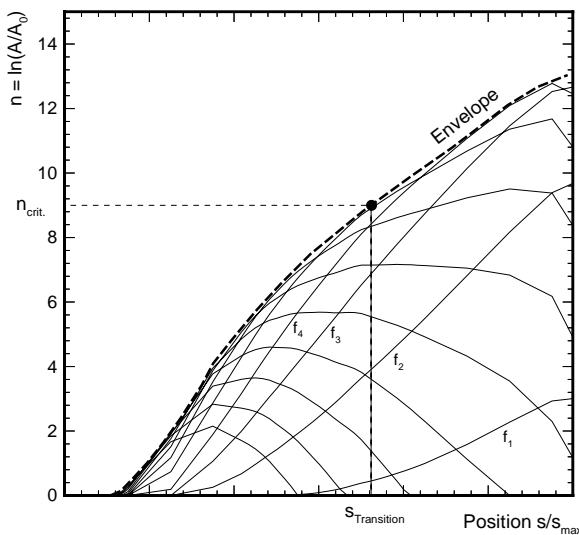


Figure 3. Amplification curves and envelope for transition prediction according to the e^n -method

Based on the shape factor H_{32l} resulting from the laminar boundary-layer calculation a Falkner-Skan profile is generated at each coordinate point in the unstable region. Then the spatial amplification rates are calculated for a multitude of physical frequencies by means of evaluating the Orr-Sommerfeld differential equation. After that, the amplification rate is integrated along the arc length of the body for each of these frequencies. Subsequently, the envelope is evaluated for the resulting amplification curves. Transition is finally assumed at the position where the envelope exceeds the specified critical value of $n_{crit.}$ (see Fig. 3). Since the boundary-layer method used does not take intermittency into account, the method switches directly from laminar to turbu-

lent boundary-layer calculation when $n_{crit.}$ is reached.

Calculating the amplification rate by solving the complete Orr-Sommerfeld equation is costly as well as problematic in highly damped regions. Therefore the analysed frequency spectrum is adjusted dynamically in the method presented here. This means that stability analysis for a specific frequency is only performed if the amplification rate $\alpha_i(f)$ is negative or the total amplification factor $n(f)$ is greater than zero. This procedure still requires too much computational effort for the purpose of numerical shape optimization because of the great number of designs to be analysed. Therefore a simplified method has been implemented, which can be used alternatively. With this method, the amplification rate for many shape factors, Reynolds numbers and frequencies is calculated by solving the Orr-Sommerfeld equations in advance. The results were stored in a data base, from which the required amplification rates can be interpolated during the actual transition calculations. For the present method a data base with 27 shape factors at 40 different Reynolds numbers and 40 different frequencies has been generated which constitutes an adequately fine discretization.

2.4 Validation of the Calculation Method

Body of Revolution with Fixed Transition

The analysis method described in the previous sections has been verified with regard to drag computation for a great number of bodies of revolution. As an example, Fig. 4 shows the calculated drag curve for Gertler body 4154 [7] which represents a shape similar to an airship hull. The theoretical drag curve is compared to results from water-tunnel tests performed by Gertler. Both, in the experimental investigation and in the theoretical computation the transition point has been fixed at 5 % of the body length. Good agreement for the whole Reynolds number range examined has been achieved.

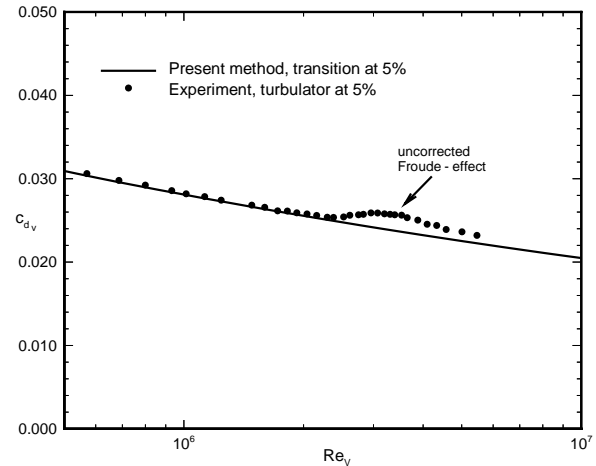


Figure 4. Inviscid pressure distribution and drag curve for Gertler body 4154 (see [7])

Body of Revolution with Natural Transition

The validation of the calculation method and especially of the transition criterion for axisymmetric bodies is difficult

since only very few experimental investigations for airship-like bodies at larger Reynolds numbers are known. In Fig. 5 experimental results of Jones resp. Schirmer [20] for the R101 airship body are depicted. These very old measurements have to be examined with caution since the then available wind tunnels featured a relatively high level of freestream turbulence. In case of the LZ wind tunnel, in which Schirmer conducted his experiments, a turbulence factor of 1.35 is referred, from which a turbulence level of approximately 0.45% can be estimated. For this turbulence level a critical amplification factor of $n_{crit.} = 5.7$ results from the correlation according to van Ingen. The theoretically obtained drag curve for that value of $n_{crit.}$ shows satisfactory agreement with the experimental results (see Fig. 5). To complement this, measurements for low Reynolds numbers are also depicted, which were determined by Jones in the wind tunnel in Teddington (see [20]). A better possibility of validating the transition criterion and

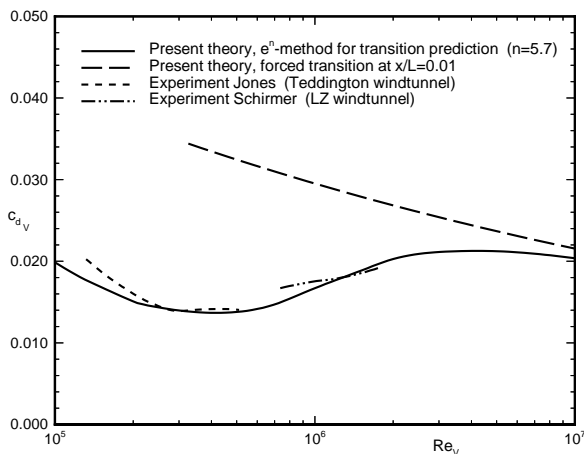


Figure 5. Inviscid pressure distribution and drag curve for R101 airship body

the boundary-layer calculation is offered by the comparison with experimental results for airfoil sections carried out in modern, low-turbulence wind tunnels. Pertinent experiments for laminar airfoil sections are available in great numbers. As an example, Fig. 6 depicts the experimentally obtained and the theoretically calculated drag polars for the sailplane airfoil section SM 701 (see [1]). When using a local transition criterion, the laminar drag bucket is determined considerably too optimistically. In contrast, a very good agreement results if the e^n -method for transition prediction as presented in this paper is utilized. Small differences at a lift coefficient of about $C_l=0.3$ probably result from laminar separation bubbles, which are not considered within the calculation.

3 Numerical Shape Optimization Procedure

3.1 Optimization Algorithm

The aerodynamical optimization problem presented is first characterized by the fact, that the gradient of the objective function (drag coefficient) can not be determined analytically. Furthermore, the objective function is expected to be multi-modal, i. e. it shows more than one minimum within the design space. The optimization algorithm must therefore be efficiently applicable to such multi-dimensional, multi-modal

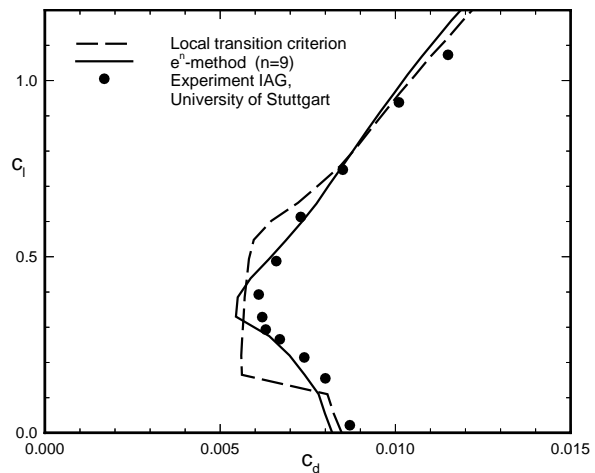


Figure 6. Drag Curve of the SM 701 airfoil section, $Re=2.5 \times 10^6$

and non-linear objective functions. In addition, the algorithm should be robust, i. e. processing of optimization problems with complex topology of the objective function should be possible. Experience shows that especially the subject last mentioned is important for shape optimizations of laminar bodies. In the vicinity of the optimum, even smallest variations of the design variables can trigger an upstream jump of the theoretical transition location. This increases the drag coefficient drastically, which is equivalent to a jump of the objective function value. When dealing with shape optimization of bodies with almost fully turbulent boundary layer, the contrary is true. In this case, large variations of the design variables only result in small changes of the drag coefficient. Such complex topologies with gorges and large plains make high demands on the step-size adaption of the optimization tool.

Various optimization strategies have been applied for the shape optimizations presented in Section 4. First, the commercially available tool POINTER was used, which enables non-linear multidimensional constrained optimization. This hybrid optimizer is made up of a combination of genetic algorithm, downhill simplex and gradient method. A search procedure suitable for the optimization task at hand is chosen by means of automated training sessions with the desired optimization time being specified. The algorithm combination chosen, the number of iterations and restarts as well as the step-sizes are not known to the user. By using stochastic methods and a great number of restarts it is possible to cover a large region of the design space if this is required. Within the present investigations, the results obtained with this tool are used as initial values for further optimization runs with an alternative strategy.

This second optimization tool is an evolution strategy with derandomized covariance matrix adaption (see [8]) implemented for a generalized individual mutation step-size control. The classical evolution strategy is an optimization method which takes reference to the biological evolution process (see [18]). Mechanisms such as recombination, random mutation and selection are adopted to generate new design vectors from a given pool of initial designs. A simple (1, 30)-selection strategy was used for the shape optimizations presented.

Of crucial importance for the success of an optimization is the self-adaptation of the step-size which is used for mutation of the design variables. In the method applied the mutation step-size is adjusted according to the selection information acquired along a whole evolution path. Aside from laying down the global step-size, this principle is also used to determine the mutation distribution, or, in other words, to determine a linear transformation of the coordinate system. This means that during the evolution process the optimization tool learns of which order of magnitude mutation step-size and direction for the individual design variables should be. The method is characterized by a high convergence rate even for complex objective functions after successful adaption of the covariance matrix.

3.2 Selection of Design Variables and Definition of the Optimization Target

Representation of the Body Shape

Contrary to the usual approach, the geometry of the body is not optimized in a direct way in the method presented here. Rather, the source distribution on the body axis is varied by the optimizer. The indirect method described in Section 2.1 is applied to calculate the corresponding body geometry and velocity distribution for each design. This procedure is essentially similar to the method of Pinebrook who performed shape optimizations of axisymmetric bodies to minimize the drag coefficient based on frontal area (see [17]).

In the investigations presented in Section 4, the lengths of the respective segments Δx_i are optimized along with the source strength q_{0_i} at the beginning of each segment and the strength at the end of the last segment q_{1_N} (compare Section 2.1). In order to prevent negative values for Δx_i , a logarithmic scale is introduced, so that the following set of design variables results:

$$q_{0_i}; \quad \log(\Delta x_i) \quad \text{with} \quad i=[1,2, \dots, N]$$

and

$$q_{1_N} \quad (9)$$

To ensure a continuous singularity distribution, the source strengths at the end of the segment boundaries q_{1_i} are not used as design variables but are set as follows:

$$q_{1_i} = q_{0_{i+1}} \quad \text{with} \quad i=[1,2, \dots, N-1] \quad (10)$$

The shape optimizations presented in Section 4 have been carried out with $N=20$ source segments, which relates to a total of 41 design variables. It should be noted that no geometric constraints are introduced within the present shape optimizations at all. This means that an arbitrary body geometry can result, with the optimization process being driven solely by the aerodynamic objective to minimize drag.

With the indirect method chosen, the closure condition has to be fulfilled in order to create closed body contours. To this end, the source distributions generated by the optimizer are superimposed by a parabolic correction distribution. Even if the closure condition is satisfied, it is possible that negative values for the source-strength integral within the singularity distribution will result. This would lead to inadmissible solutions. Such designs are therefore eliminated or avoided by introducing proper constraints.

Optimization Target and Objective Function

The optimization target relevant for the aerodynamic design of airship hulls is to achieve minimum drag at specified hull volume and airspeed (compare [11], [19]). During the investigation of this question the following dimensionless quantities are relevant when comparing different configurations:

Volumetric drag coefficient:

$$c_{d_V} = \frac{D}{\frac{\rho}{2} U_\infty^2 V^{2/3}} \quad (11)$$

Volumetric Reynolds number:

$$Re_V = \frac{U_\infty V^{1/3}}{\nu} \quad (12)$$

With airships, the span of the volumetric Reynolds number extends from $Re_V \approx 5 \cdot 10^6$ for the unmanned solar airship 'Lotte' up to $Re_V \approx 150 \cdot 10^6$ for the Zeppelin LZ 129 (in each case at maximum speed). An inconsistent choice of the reference length, e. g. airship length for the Reynolds number and $V^{1/3}$ for the drag coefficient, leads to wrong results if drag coefficients for different configurations are compared.

In order to realize the above mentioned optimization target, the volumetric drag coefficient at a specified volumetric Reynolds number was chosen as the objective function to be minimized in the optimization runs presented. To enable shape optimizations for a broader airspeed region, the present optimization tool also allows to specify a weighted mean value of c_{d_V} for a whole Reynolds number region as objective function.

The total drag coefficient defining the fitness comprises friction and form drag of the attached boundary layer as well as a penalty function representing the pressure drag if turbulent separation occurs. Because the last mentioned drag portion cannot be calculated to a high degree of accuracy and reliability, a pessimistic penalty function was chosen. During the optimization process this yields body shapes with negligible separated flow region.

4 Results and Discussion

When plotting the drag coefficient of an axisymmetric body versus Reynolds number, three different regions can be distinguished. At low Reynolds numbers ($Re_V \lesssim 5 \cdot 10^6$), extensive laminar flow is possible which results in low skin friction. With increasing Reynolds number the transition point moves more or less rapidly towards the body nose, thereby increasing the drag coefficient (see Fig. 5). The large Reynolds number regime ($Re_V \gtrsim 10^7$) can be characterized by the fact that the boundary layer is almost fully turbulent.

An important task of aerodynamics is to determine how to shape the body geometry to delay transition and to realize extensive laminar flow. This question has been examined for different Reynolds number regimes by application of the optimization tool described in the previous section. The calculations were performed assuming natural boundary-layer transition. However, it is not known to what extent the theoretically evaluated laminar flow can be realised with actual airship applications with a certain degree of surface waviness.

For the shape optimizations presented in [14], it became obvious that one-point optimizations for a single Reynolds number lead to bodies which are inconvenient or even unusable outside of their design point. This is especially true for

laminar bodies at low Reynolds numbers. For this reason, the shape optimizations presented hereafter were performed for a whole Reynolds number regime. Because the practical value of optimized laminar bodies is to a large extent dependent on the quality and reliability of the transition criterion, the costly e^n -method was applied for transition prediction. Four design regimes were chosen, which cover the whole Reynolds number regime relevant for airship applications:

$$\begin{aligned} \text{Design regime I:} \quad & Re_{V_I} = 1 \cdot 10^6 \dots 3.16 \cdot 10^6 \\ & (6 \leq \log Re_{V_I} \leq 6.5) \end{aligned}$$

$$\begin{aligned} \text{Design regime II:} \quad & Re_{V_{II}} = 3.16 \cdot 10^6 \dots 1 \cdot 10^7 \\ & (6.5 \leq \log Re_{V_{II}} \leq 7) \end{aligned}$$

$$\begin{aligned} \text{Design regime III:} \quad & Re_{V_{III}} = 1 \cdot 10^7 \dots 3.16 \cdot 10^7 \\ & (7 \leq \log Re_{V_{III}} \leq 7.5) \end{aligned}$$

$$\begin{aligned} \text{Design regime IV:} \quad & Re_{V_{IV}} = 3.16 \cdot 10^7 \dots 1 \cdot 10^8 \\ & (7.5 \leq \log Re_{V_{IV}} \leq 8) \end{aligned}$$

The initial source distribution chosen for design regime I corresponded to an ellipsoid-like starting geometry with a small length-to-diameter ratio of $L/D=2.3$. At first, an optimization run with the commercially available tool POINTER was carried out. Positive values for the source-strength integral at the segment boundaries were prescribed as constraints. Within the transition calculation, a critical amplification factor of $n_{crit.} = 9$ was chosen, which corresponds to a moderate level of turbulence in the freestream.

The optimization result obtained with POINTER was used as initial vector for a further optimization run with the evolution strategy with derandomized covariance matrix adaption. In this process, designs in the order of 200,000 were generated and analysed during each optimization run. Fig. 7 shows the

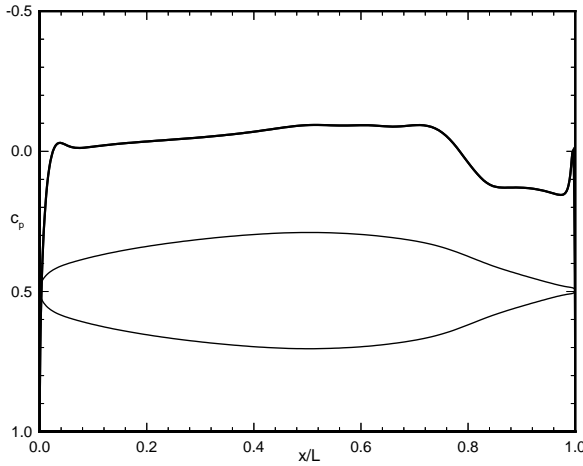


Figure 7. Inviscid pressure distribution of the body optimized for design regime I ($Re_{V_I} = 1 \cdot 10^6 \dots 3.16 \cdot 10^6$)

contour and the inviscid pressure distribution of the superior result from both optimization runs for design regime I. This relatively slender body is characterized by its far aft position of the maximum thickness point and by moderate, almost constant acceleration upstream of this point. This slightly favorable pressure gradient is sufficient to keep the boundary

layer laminar up to 75% of the body length at Reynolds numbers below $Re_V = 3.16 \cdot 10^6$. Downstream of transition the body shows a steep pressure rise. This corresponds to a reduction in diameter and a reduction of the wetted surface area in the region of high turbulent skin friction values. The resulting drag curve for the optimized body is shown in Fig. 8. Very low drag coefficients for the whole design regime can be observed. However, if the Reynolds number is only slightly increased above the design region, transition will jump upstream causing an abrupt drag increase. Below $Re_V = 1 \times 10^6$ laminar separation without reattachment is indicated. The drag curve is not plotted for this regime.

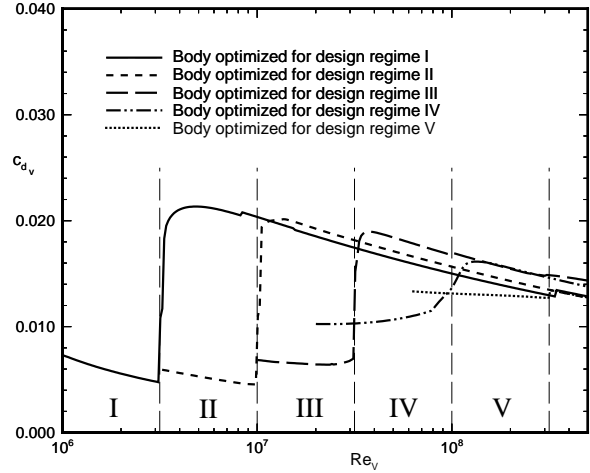


Figure 8. Drag curve of the optimized body shapes

An interesting phenomena can be observed for the optimized body: When comparing body contour and pressure distribution in Fig. 7, it becomes obvious that the minimum pressure coefficient occurs downstream of the maximum thickness point. Therefore within the design Reynolds number regime, body contraction has started upstream of transition. In consequence, the high turbulent skin friction acts on a smaller wetted surface area thus reducing the viscous drag of the body.

With an increase in Reynolds number the amount of favorable pressure gradient in the forebody region has to be enlarged in order to maintain laminar flow. This can be realized either by increasing the body diameter or by moving the maximum thickness point upstream. Enlarging the body diameter is limited by the maximum pressure recovery possible without boundary-layer separation arising in the rear part of the body. On the whole, one has to expect smaller laminar flow regions and bodies with a smaller length-to-diameter ratio when increasing the design Reynolds number. The compromise found with the optimization tool for design regime II can be seen in Fig. 9. The resulting body again shows a very low drag coefficient and extensive laminar flow regions for the whole design region (see Fig. 8).

With the body optimized for design regime III a further upstream movement of the transition point and a further reduction of the fineness ratio can be observed. A steep favorable pressure gradient during the first 50 % of the body length is required to achieve extensive laminar flow by shaping alone.

A somewhat unusual body shape finally results for design regime IV, see Fig. 11. The gradient of the pressure coefficient

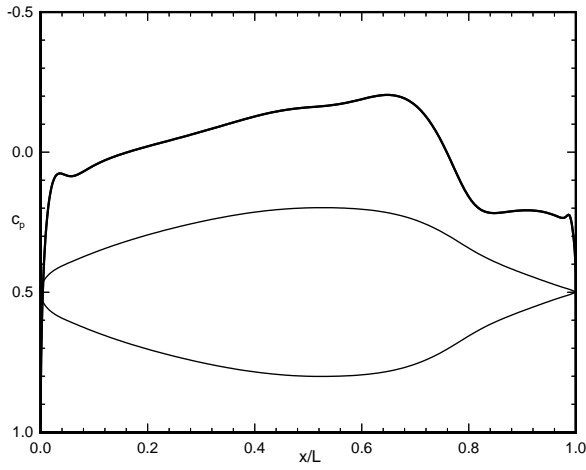


Figure 9. Inviscid pressure distribution of the body optimized for design regime II ($Re_{V,II}=3.16 \cdot 10^6 \dots 1 \cdot 10^7$)

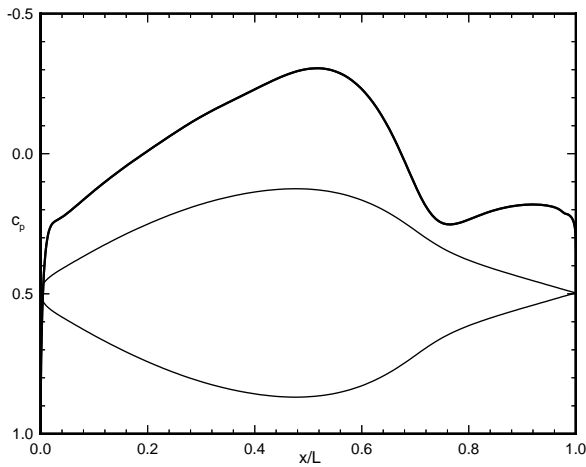


Figure 10. Inviscid pressure distribution of the body optimized for design regime III ($Re_{V,III}=1 \cdot 10^7 \dots 3.16 \cdot 10^7$)

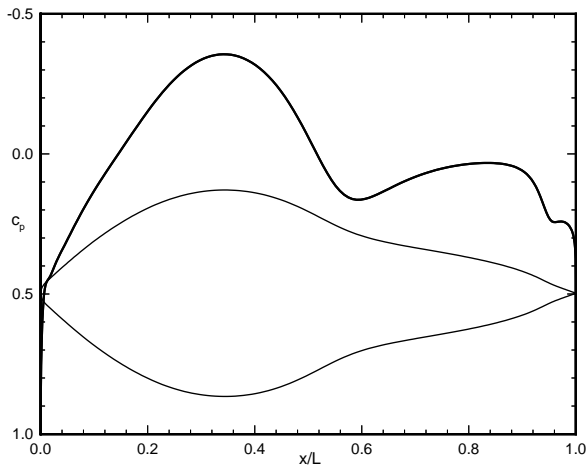


Figure 11. Inviscid pressure distribution of the body optimized for design regime IV ($Re_{V,IV}=3.16 \cdot 10^7 \dots 1 \cdot 10^8$)

in the nose region is increased once more and the maximum thickness position is moved further upstream. At the upper end of the design regime ($Re_V=10^8$) the calculated transition point already moves noticeably upstream. The value of the objective function (arithmetic mean value of the drag coefficients for six different Reynolds numbers) is obviously minimized, if a movement of the transition point at $Re_V=10^8$ is accepted in exchange for longer laminar flow regions at lower Reynolds numbers.

In contrast, a body optimized for a single Reynolds number of $Re_V=10^8$ while employing a local transition criterion has an entirely different shape, see [14]. The volumetric drag coefficient at a specified volumetric Reynolds number is very insensitive to changes in shape if the boundary layer is turbulent over almost the entire length of the body [10]. The drag coefficient at these high Reynolds numbers can only be significantly reduced if the nose region is shaped such that a certain level of laminar flow is achieved. This is the reason why the transition criterion used has a great influence on the shape of the forebody region.

Finally, an optimization run for huge Reynolds numbers was performed at reduced optimization time:

$$\text{Design regime V: } Re_{V,V}=1 \cdot 10^8 \dots 3.16 \cdot 10^8 \\ (8 \leq \log Re_{V,V} \leq 8.5)$$

The contour and the inviscid pressure distribution of the resulting, not completely optimized body are shown in Fig. 12. An extremely steep favorable pressure gradient at the nose region theoretically allows for laminar flow up to 17% body length even at the upper end of the design regime. The resulting shape shows an almost pointed nose similar to the body presented in [14]. However, it is to be noted that for small angles of attack or sideslip the transition point is expected to move upstream more rapidly than in case of blunt nose shapes.

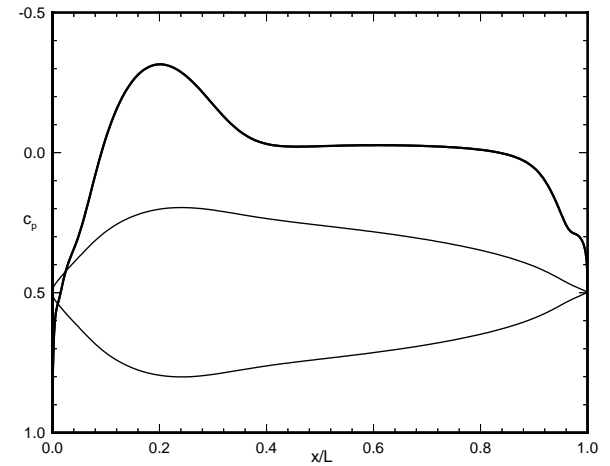


Figure 12. Inviscid pressure distribution of the body optimized for design regime V ($Re_{V,V}=1 \cdot 10^8 \dots 3.16 \cdot 10^8$)

Drag curves for all optimized bodies are summarized in Fig. 8. It can be seen that the bodies only show favorable behaviour inside their respective design regimes. Exact information about the design Reynolds number regime is therefore of crucial importance especially for the selection of laminar body shapes. It is still not known in how far the theoretically

calculated laminar flow regions can be realized in practical airship applications if the existence of surface roughness and waviness is considered. Relevant investigations are still to be done.

5 Summary and Outlook

A method for numerical shape optimization of axisymmetric bodies at zero incidence submerged in incompressible flow was developed and has been presented here. This tool allows specific aerodynamic optimization of bodies of revolution for prescribed Reynolds number regimes. Using this method, several bodies, which show minimized drag at maximized volume were designed for the Reynolds number regime relevant for airship application. Although it is not known in how far laminar flow can be realized if the surface waviness of real airships is considered, the optimizations were carried out assuming natural transition. A semi-empirical e^n -method has been used for transition prediction within the optimization process for the first time. This costly method was used because earlier investigations had shown that simpler local criteria are too unreliable for optimization purposes.

The results show that up to large, airship-relevant Reynolds numbers a certain amount of laminar flow is theoretically possible by adequate shaping of the body contour. The calculation results still have to be validated experimentally. Especially it has to be investigated how surface irregularities of real airship hulls affect the transition location. Corresponding in-flight investigations are planned to be performed at the University of Stuttgart with an unmanned airship.

The optimization tool presented will be used in the future for the shape optimization of airship hulls which will take the drag of the required tail surfaces into account. It will also be possible to consider other constraints important for a specific airship design, such as hull mass minimization or prescription of a desired center of buoyancy. Finally, implementation of the propeller model presented in [12] should enable aerodynamic optimization of complete airship configurations.

Acknowledgement

The authors wish to thank N. Hansen of Berlin Technical University for providing the optimization algorithm and for his helpful support in conducting the present optimization runs.

REFERENCES

- [1] D. Althaus. *Niedriggeschwindigkeitsprofile*. Friedrich Vieweg & Sohn Verlagsgesellschaft mbH, Braunschweig/Wiesbaden, 1996. ISBN 3-528-03820-9.
- [2] Bruce H. Carmichael. *Underwater Drag Reduction Through Optimum Shape*. AIAA Second Propulsion Joint Specialist Conference, Colorado Springs, Colorado, June 13–17, 1966.
- [3] D. P. Coiro and F. Nicolosi. *Design of Natural Laminar Flow Fuselages*. ICAS-94-4.7.4.
- [4] S. S. Dodbele, C. P. van Dam, P. M. H. W. Vijgen, and B. J. Holmes. *Shaping of Airplane Fuselages for Minimum Drag*. AIAA Paper 86-0316 (1986).
- [5] S. S. Dodbele. *Design Optimization of Natural Laminar Flow Bodies in Compressible Flow*. J. Aircraft, Vol. 29, No. 3, May-June 1992.
- [6] R. Eppler and D. M. Somers. *A Computer Program for the Design and Analysis of Low-Speed Airfoils*. NASA TM 80210 (1980).
- [7] Morton Gertler. *Resistance Experiments on a Systematic Series of Streamlined Bodies of Revolution - for Application to the Design of High Speed Submarines*. Navy Department, Report C-297, April 1950; Central Air Documents Office, Wright Patterson Air Force Base, Dayton, Ohio.
- [8] N. Hansen and A. Ostermeier. *Adapting arbitrary normal mutation distributions in evolution strategies: The covariance matrix adaptation*. Proceedings of the 1996 IEEE International Conference on Evolutionary Computation, May 20–22, 1996, Nagoya, Japan.
- [9] R. J. Hansen and J. G. Hoyt. *Laminar-To-Turbulent Transition on a Body of Revolution with an Extended Favorable Pressure Gradient Forebody*. Journal of Fluids Engineering, Vol. 106, June 1984, pp. 202–210 (1984).
- [10] John L. Hess and R. M. James. *On the problem of shaping an axisymmetric body to obtain low drag at large Reynolds numbers*. Douglas Aircraft Company, Long Beach, CA, Report MDC J6791, January 1975.
- [11] C. K. Lavan and C. K. Drummond. *Applications of Similitude in Airship Design*. J. of Aircraft, Vol. 24, No. 4, April 1987, pp. 287–288 (1987).
- [12] Th. Lutz, D. Leinhos, and S. Wagner. *Theoretical Investigations of the Flowfield of Airships with a Stern Propeller*. International Airship Convention and Exhibition; Bedford, Great Britain, 5–7 July 1996.
- [13] Th. Lutz, U. Rüger, and S. Wagner. *Theoretische Untersuchungen zur Minimierung des aerodynamischen Widerstandes von Luftschiffrümpfen*. DGLR Fachausschusstagung S 2.3, Dresden, 25.9.1996.
- [14] Th. Lutz, H. Schweyher, S. Wagner, and R. Bannasch. *Shape Optimization of Axisymmetric Bodies in Incompressible Flow: Results for the High Reynolds Number Regime*. 2nd International Airship Conference, Stuttgart/Friedrichshafen, 3–4 July 1996.
- [15] L. M. Mack. *A numerical method for the prediction of high-speed boundary-layer transition using linear theory*. NASA SP-347, 1975.
- [16] Jerome S. Parsons and Raymond E. Goodson. *Shaping of Axisymmetric Bodies for Minimum Drag in Incompressible Flow*. J. Hydronautics, Vol. 8, No. 3 (1974).
- [17] William Edward Pinebrook. *Drag Minimization on a Body of Revolution*. Dissertation at the Faculty of the Department of Mechanical Engineering of the University of Houston (1982).
- [18] Ingo Rechenberg. *Evolutionsstrategie '94 - Werkstatt Bionik und Evolutionstechnik, Band 1*. Frommann-Holzboog Verlag, Stuttgart (1994).
- [19] U. Rüger and B. Kröplin. *Aim of Airship Drag Reduction and Evaluation Method*. 2nd International Airship Conference, Stuttgart/Friedrichshafen, 3–4 July 1996.
- [20] Max Schirmer. *Aerodynamische Modellversuche an deutschen und ausländischen Luftschiff-Baumustern im Windkanal des Luftschiffbau Zeppelin in Friedrichshafen*. Dissertation an der Technischen Hochschule Carolo-Wilhelmina zu Braunschweig (1942).
- [21] A. M. O. Smith and N. Gamberoni. *Transition, Pressure Gradient and Stability Theory*. Douglas Report No. ES 26388 (1956).
- [22] J. L. van Ingen. *A Suggested Semi-Empirical Method for the Calculation of the Boundary Layer Transition Region*. Report Nos. V.T.H. 71, V.T.H. 74, Delft (1956).
- [23] J. L. van Ingen and L. M. M. Boermans. *Research on Lam-*

inar Separation Bubbles at Delft University of Technology in Relation to Low Reynolds Number Airfoil Aerodynamics. Department of Aerospace Engineering, Delft University of Technology, The Netherlands.

- [24] H. Schweyher; Th. Lutz; S. Wagner. *An Optimization Tool for Axisymmetric Bodies of Minimum Drag*. 2nd International Airship Conference, Stuttgart/Friedrichshafen, 3-4 July 1996.
- [25] Werner Würz. *Hitzdrahtmessungen zum laminar-turbulenten Strömungsumschlag in anliegenden Grenzschichten und Ablöseblasen sowie Vergleich mit der linearen Stabilitätstheorie und empirischen Umschlagskriterien*. Dissertation, Institut für Aerodynamik und Gasdynamik, Universität Stuttgart (1994).
- [26] A. D. Young. The calculation of total and skin friction drags of bodies of revolution at zero incidence. ARC R&M No. 1874 (1939).
- [27] M. F. Zedan. *Flow Around Axisymmetric Bodies, The Direct and Inverse Problems*. Ph.D. Dissertation, University of Houston, 1979.
- [28] M. F. Zedan, A. A. Seif, and S. Al-Moufadi. *Drag reduction of airplane fuselages through shaping by the inverse method*. Journal of Aircraft, Vol. 31, No. 2, March-April 1994.